Electric Torque Vectoring Driveline Technology Assessment via Bond Graph Modeling and Simulation

Jose Velazquez Alcantar[1]
Ming Kuang[2]
Research and Innovation Center
Ford Motor Company
Dearborn, MI 48124, USA
jose.velazquez@ford.com[1], mkuang@ford.com[2]

***Abstract*— With the push for vehicle electrification in full swing, many automotive manufacturers are currently launching their first generation battery electric vehicles (BEV). Many of these BEVs use simple driveline configurations such as single speed gearboxes with open differentials. In an effort to further advance the handling capabilities of these vehicles, automotive manufacturers are looking into recent electric torque vectoring (eTV) technology enhancements. This paper analyzes three key eTV technologies and uses bond graphs to assess the pros and cons of each technology via modeling and simulation. The first of these eTV concepts is the independent motor design where an independent motor drives each wheel on the axle. Next, we consider a super positioning eTV concept that allows the vectoring torque to act independently of the traction torque. Lastly, a twin clutch eTV design is analyzed which uses two clutch packs to deliver the traction motor torque to the drive wheels. An open differential with brake-based torque vectoring is considered as the baseline for the analysis. Bond graph models are derived for each eTV concept and they are compared to one another in the simulation environment with a correlated high-fidelity CarSim vehicle dynamics model. The power limitation of electric motors is included in the assessment in order to have a fair comparison and it is found that the super positioning eTV concept offers the strongest balance of performance and expected cost for on-road vehicles.**

I. Introduction

Torque vectoring technology has been readily found on performance oriented conventional vehicles for quite some time now. The two most common forms of passive torque vectoring technologies are torque vectoring by brake [1], [2] and limited slip differentials (LSD). In order to further expand the yaw control performance, several active torque vectoring technologies have been developed such as electric limited slip differentials (eLSD) and multi-clutch pack devices [3] that allow for greater control of the torque biasing across the axle. Although these active systems allow for greater torque biasing control, they can only distribute the input torque from the engine. Here is where vehicle electrification can push the boundary even further.

Electrified powertrains have greater torque control capability depending on the driveline topology. The BEV powertrain architecture has the flexibility of using multiple motors and gearbox designs to achieve the electric torque vectoring (eTV) functionality. It has been shown that electric torque vectoring can drastically improve the handling performance of the vehicle [4], [5]. However, the torque vectoring capability of a BEV greatly depends on the driveline topology. This paper presents a study on three eTV technologies and how each topology affects the eTV capability. The study relies on the bond graph modeling methodology [6] to create mathematical models for simulation analysis. The first of the eTV technologies is a dual motor design that uses two independent motors to power each wheel on the axle. A superpositioning system is also analyzed which uses a clever gearbox design to super position the vectoring torque on top of the traction torque. Finally, a twin clutch design is considered which uses a pair of clutch packs to achieve the traction and vectoring torque functionality. The three eTV systems are also compared to a brake torque vectoring system with an electrified open differential. Bond graph models of all the systems are presented and analyzed in the simulation environment with a high fidelity vehicle dynamics model.

II. Driveline Modeling

The vehicle configuration for this study is the electric All-Wheel-Drive (eAWD) BEV shown in fig. 1. As can be seen, the front and rear axles are mechanically decoupled. The front axle is powered by an eAxle with an open differential, the rear axle is powered by an eTV axle. The axles are powered by the energy stored in the high voltage battery. This vehicle configuration allows the vehicle dynamics controller to adjust the torque split between the front and rear axle and between the left and right wheels on the rear axle. The main focus of this study is how different eTV axle configurations affect the vehicle dynamics. As such, four different eTV configurations are considered. First a baseline is defined as an eAxle with an open differential and brake torque vectoring. The first of the eTV concepts is a twin motor design with one motor powering each wheel on the rear axle. For the sake of brevity, we will label this system as ”Type A”. Next, a superpositioning system is introduced which uses a traction motor and a small vectoring motor with decoupled behavior to power the rear wheels; we label this system as ”Type B”. Finally, a twin clutch design is presented which uses a pair of clutch packs to distribute the traction motor torque between the left and right wheels; we will label this system as ”Type C”. Bond graphs

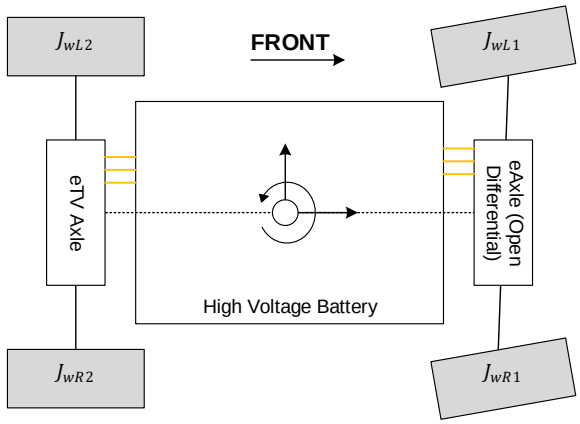

Fig. 1: eAWD BEV configuration with eTV axle

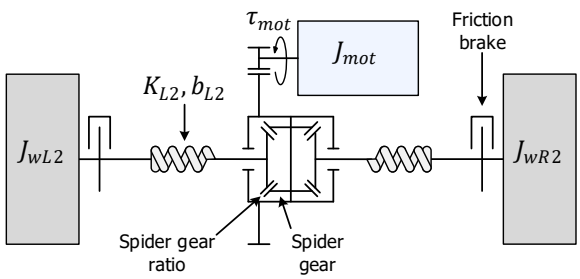

Fig. 2: Diagram of open differential with torque vectoring by brake

models of each configuration are presented in the following subsections. The bond graph modeling methodology allows for an intuitive graphical modeling approach from which first order differential equations of motion can be easily derived from [6].

A. Brake Torque Vectoring with Open Differential

The baseline for the analysis is torque vectoring via friction brakes on an open differential. This is the most common form of torque vectoring and is readily found on many production vehicles [1], [2]. Figure 2 shows a diagram of an open differential powered by an electric motor with a friction brake on each wheel. This driveline configuration is the most economical solution and thus the most common in production vehicles. An open differential will always split the input torque evenly between the two halfshafts [7]. However, if one wheels slips, the torque capability of the entire axle is limited to the wheel with the lowest grip. Thus, individual friction brake torque must be applied in order to transfer torque to the high μ side. The basis for torque vectoring by brake is to actuate individual friction brakes in order to produce the desired yaw moment. Although effective, this approach can be quite jarring to the driver due to the accuracy of pressure control from the brakes and slowing the vehicle down. However, with the proper coordination between powertrain and friction brake torque, a smooth yaw moment response can be achieved and this is the strategy that is adopted for this study.

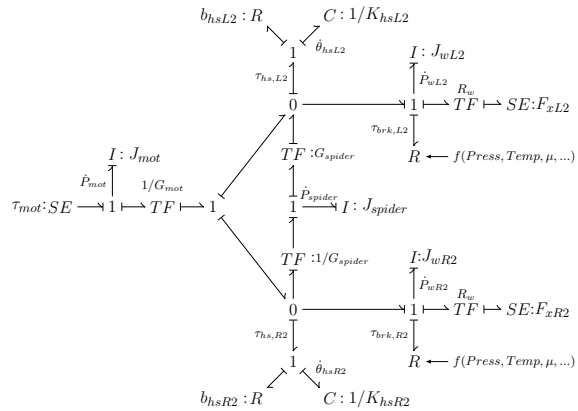

Fig. 3: Bond graph model of brake torque vectoring with open differential

The bond graph model for this system is given in fig. 3. The input motor torque is multiplied by the gear ratio G_{mot} before it is applied to the differential carrier. Note that the spider gear is modeled as it's own inertia in order to capture the loss of traction across the axle when one wheel looses grip. The spider gear is responsible for the differential action by balancing the load between the two halfshafts and the differential carrier. When one wheel slips, the input energy chooses the path of least resistance and spins up the spider gear thus reducing the torque capability of the entire axle to the friction capability of the slipping wheel. The kinematic constraint of the spider gear is derived as

$$\omega_{LeftSideGear} = \omega_{ring} + \omega_{spider} G_{spider} \tag{1}$$

$$\omega_{RightSideGear} = \omega_{ring} - \omega_{spider} G_{spider} \tag{2}$$

The spider gear ratio is the gear ratio between the spider and side gears. Moreover, each halfshaft is modeled as a spring damper system. Finally, the friction brakes are modeled as modulated resistance elements and the friction brake torque is applied directly to each wheel. The equations of motion for this system are derived as:

$$J_{mot}\dot{\omega}_{mot} = \tau_{mot} - \frac{1}{G_{mot}}\left(\tau_{hs,L2} + \tau_{hs,R2}\right) \tag{3}$$

$$J_{spider}\dot{\omega}_{spider} = G_{spider}\left(\tau_{hs,R2} - \tau_{hs,L2}\right) \tag{4}$$

$$\dot{\theta}_{hs,L2} = \frac{\omega_{mot}}{G_{mot}} + G_{spider}\omega_{spider} - \omega_{w,L2} \tag{5}$$

$$\dot{\theta}_{hs,R2} = \frac{\omega_{mot}}{G_{mot}} - G_{spider}\omega_{spider} - \omega_{w,R2} \tag{6}$$

$$J_w\dot{\omega}_{w,i2} = \tau_{hs,i2} - \tau_{brk,i2} - R_w F_{x,i2} \quad i \in \{L, R\} \tag{7}$$

$$\tau_{hs,i2} = K_{hs}\theta_{hs,i2} + b_{hs}\dot{\theta}_{hs,i2} \quad i \in \{L, R\} \tag{8}$$

$$\tau_{brk,ij} = f(\omega_{w,i2}, pressure, temp, \mu, ...) \quad i \in \{L, R\} \tag{9}$$

Note that in eq. (9) the friction brake torque is a nonlinear function of wheel speed, brake line control pressure, and brake pad friction among other variables. The friction brakes are modeled in CarSim and include fluid dynamics, thermal dynamics, and friction changes [8]. The friction brake model

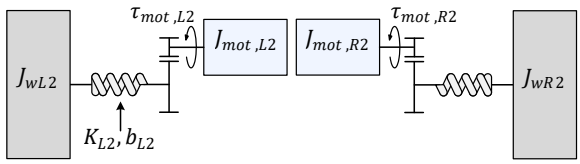

Fig. 4: Diagram of twin motor system (Type A)

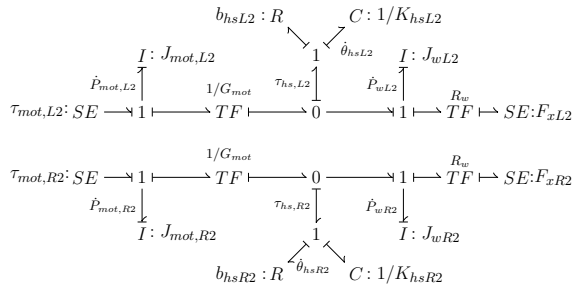

Fig. 5: Bond graph model of twin motor system (Type A)

captures the change in friction brake torque as a function of rotor temperature which is an important effect to be considered in brake torque vectoring. The same open differential model is used to power the front axle of the vehicle for this study but without the brake torque vectoring capability.

B. Twin Motor System (Type A)

The first of the eTV concepts considered in this study is the twin motor design nicknamed "Type A" shown in fig. 4. As can be seen, this system uses a pair of traction motors to power the rear wheels. Each motor has a single speed gearbox and powers an individual wheel. This type of system offers the most flexibility in wheel torque control due to the fact that each wheel is powered by an independent motor. The biggest disadvantage of such a system is cost since this system requires two large traction motors, gearboxes and inverters.

The bond graph model for the Type A system is shown in fig. 5. As can be seen, each motor is independent of the other. The single speed gearboxes are modeled as an ideal gear reduction without losses. The halfshafts are modeled as spring damper systems. The state equations can be derived from this model as:

$$J_{mot}\dot{\omega}_{mot,L2} = \tau_{mot,L2} - \frac{\tau_{hs,L2}}{G_{mot}} \tag{10}$$

$$J_{mot}\dot{\omega}_{mot,R2} = \tau_{mot,R2} - \frac{\tau_{hs,R2}}{G_{mot}} \tag{11}$$

$$\dot{\theta}_{hs,L2} = \frac{\omega_{mot,L2}}{G_{mot}} - \omega_{w,L2} \tag{12}$$

$$\dot{\theta}_{hs,R2} = \frac{\omega_{mot,R2}}{G_{mot}} - \omega_{w,R2} \tag{13}$$

$$J_w\dot{\omega}_{w,i2} = \tau_{hs,i2} - R_w F_{x,i2} \quad i \in \{L, R\} \tag{14}$$

$$\tau_{hs,i2} = K_{hs}\theta_{hs,i2} + b_{hs}\dot{\theta}_{hs,i2} \quad i \in \{L, R\} \tag{15}$$

C. Superpositioning System (Type B)

The superpositioning eTV concept, nicknamed Type B, is shown in fig. 6. The main traction motor is placed between

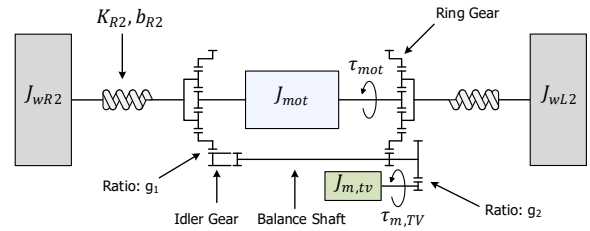

Fig. 6: Diagram of superpositioning system (Type B)

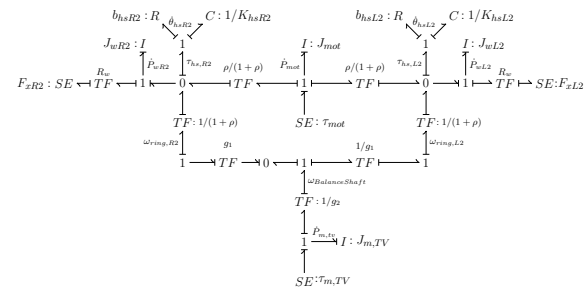

Fig. 7: Bond graph model of superpositioning system (Type B)

two planetary gearsets and powers the sun gear in each of the gear sets. The carrier of each planetary gear is connected to the halfshaft of each wheel. The ring gears are connected together via a balance shaft and an idler gear. Note that the idler gear does not introduce a gear ratio, but simply changes the direction of rotation to the R2 wheel. Finally, the small torque vectoring motor is geared directly to the balance shaft.

During straight line driving, the ring gear and balance shaft remain stationary and thus the two wheels move forward at the same speed. During cornering, the balance shaft rotates to balance the speeds of the ring gears and thus allows for differential action i.e. the two wheels can have independent speeds. Note that the torque vectoring (TV) motor is geared directly to the balance shaft. Therefore, applying a torque on the TV motor will directly change the speed of the ring gears. Thus, the TV motor can add wheel torque to the wheels, in equal and opposite quantities, based on the direction of torque application. In summary, the traction motor provides equal torque to the left and right half shafts, acting as an open differential, while the TV motor adds equal and opposite wheel torque to the left and right half shafts - the vectoring functionality is independent of the traction torque. Moreover, since the TV motor adds equal and opposite torques to the left and right halfshafts, a torque difference on the rear axle is created while the net wheel torque does not change; therefore, the torque vectoring functionality has minimal impact on the longitudinal velocity of the vehicle. The bond graph model for the Type B system is given in fig. 7.

In Figure 7, g_1 represents the gear ratio from the balance shaft to the ring gears whereas g_2 is the TV gear ratio to the balance shaft. Note that the zero junction to the left of the $\omega_{BalanceShaft}$ one junction represents the idler gear - the sign of the speed changes while maintaining the same torque. The dynamic equations for this system are derived

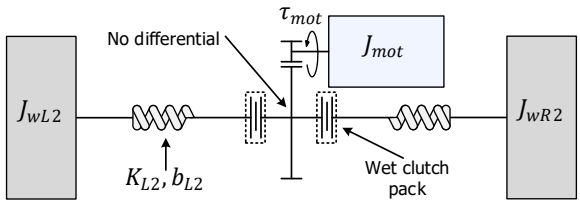

Fig. 8: Diagram of twin clutch system (Type C)

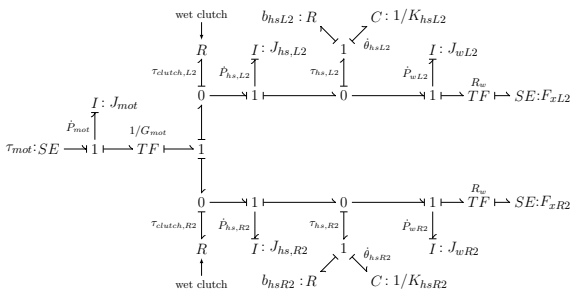

Fig. 9: Bond graph model of twin clutch system (Type C)

as:

$$J_{mot}\dot{\omega}_{mot} = \tau_{mot} - \frac{\rho}{1+\rho}(\tau_{hsL2} + \tau_{hsR2}) \tag{16}$$

$$J_{m,TV}\dot{\omega}_{m,TV} = \tau_{m,TV} - \frac{1}{g_1 g_2(1+\rho)}(\tau_{hsL2} - \tau_{hsR2}) \tag{17}$$

$$\dot{\theta}_{hsL2} = \frac{\rho}{1+\rho}\omega_{m,erad} + \frac{1}{g_1 g_2(1+\rho)}\omega_{m,TV} - \omega_{w,L2} \tag{18}$$

$$\dot{\theta}_{hsR2} = \frac{\rho}{1+\rho}\omega_{m,erad} - \frac{1}{g_1 g_2(1+\rho)}\omega_{m,TV} - \omega_{w,R2} \tag{19}$$

$$J_w\dot{\omega}_{w,i2} = \tau_{hs,i2} - R_w F_{x,i2} \quad i \in \{\text{L,R}\} \tag{20}$$

$$\tau_{hs,i2} = K_{hs}\theta_{hs,i2} + b_{hs}\dot{\theta}_{hs,i2} \quad i \in \{L, R\} \tag{21}$$

D. Twin Clutch System (Type C)

The third and final eTV concept considered in this study is the twin clutch system nicknamed Type C shown in fig. 8. This system uses one main traction motor and a single speed gearbox. Note that there is no differential in the design. Instead, a pair of wet clutch packs are used to distribute the traction motor torque between the left and right halfshafts. The clutch packs are controlled to provide the appropriate amount of torque to each wheel. It is important to note that the clutch packs are designed as slipping clutches since they will need to constantly slip in order to provide the differential action when the vehicle is turning. The clutch packs can also lock thus providing a solid locked axle if needed. This type of system also allows for all of the traction torque to be distributed to a single wheel by locking the appropriate clutch pack and opening the other. The bond graph model for the Type C system is shown in fig. 9.

As fig. 9 shows, the clutch packs are modeled as modulated resistive elements and the halfshafts are modeled as spring damper systems. For this study, the clutch torque is modeled as linear friction where the appropriate clutch torque is achieved by actively controlling the friction coefficient for each clutch, b_{clutch}. The simple linear friction model is deemed appropriate for this study since we are more interested in the vehicle level response of the eTV system rather than a driveline level analysis. Finally, the halfshafts are modeled with inertia in order to maintain the desired causality for the clutch torque. The equations of motion for the Type C system are derived from the bond graph model as:

$$J_{mot}\dot{\omega}_{mot} = \tau_{mot} - \frac{1}{G_{mot}}(\tau_{clutch,L2} + \tau_{clutch,R2}) \tag{22}$$

$$J_{hs,L2}\dot{\omega}_{hs,L2} = \tau_{clutch,L2} - \tau_{hs,L2} \tag{23}$$

$$J_{hs,R2}\dot{\omega}_{hs,R2} = \tau_{clutch,R2} - \tau_{hs,R2} \tag{24}$$

$$\dot{\theta}_{hs,L2} = \omega_{hs,L2} - \omega_{w,L2} \tag{25}$$

$$\dot{\theta}_{hs,R2} = \omega_{hs,R2} - \omega_{w,R2} \tag{26}$$

$$J_w\dot{\omega}_{w,i2} = \tau_{hs,i2} - R_w F_{x,i2} \quad i \in \{\text{L,R}\} \tag{27}$$

$$\tau_{clutch,i2} = b_{clutch,i2}\left(\frac{\omega_{mot}}{G_{mot}} - \omega_{hs,i2}\right) \quad i \in \{\text{L,R}\} \tag{28}$$

$$\tau_{hs,i2} = K_{hs}\theta_{hs,i2} + b_{hs}\dot{\theta}_{hs,i2} \quad i \in \{L, R\} \tag{29}$$

III. Simulation Analysis

The bond graph models of the eTV systems are used in simulation in conjunction with a high fidelity vehicle dynamics model from CarSim for simulation analysis. In this section, we detail the simulation environment and two simple simulation use cases that will help expose the strengths and weaknesses of the different eTV technologies.

A. Simulation Environment

The simulation environment for this study is shown in fig. 10. The causality between the driveline models and the CarSim vehicle dynamics model is such that the driveline models provide the halfshaft torque to the CarSim vehicle model and the vehicle model sends back the wheel speeds to the driveline models. As such, the CarSim vehicle model handles the wheel dynamics and tire model. Additionally, the driveline models for the rear axle also provide individual brake pressure requests to the CarSim vehicle model. The CarSim model uses the internal brakes plant model to generate the appropriate brake torque. The CarSim brakes plant model includes actuator dynamics and rotor temperature effects to determine the brake torque for a given pressure request. Finally, the CarSim vehicle model uses a validated Pacejka tire model [9].

In order to provide a fair comparison between all of the eTV technologies, the systems are sized to meet the following requirements for the rear axle:

1) The total axle traction torque shall not exceed 2000 Nm
2) The total axle traction power shall not exceed 120 kW

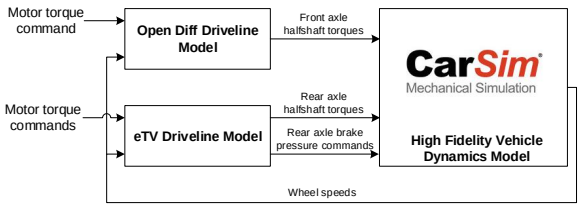

Fig. 10: Simulation environment

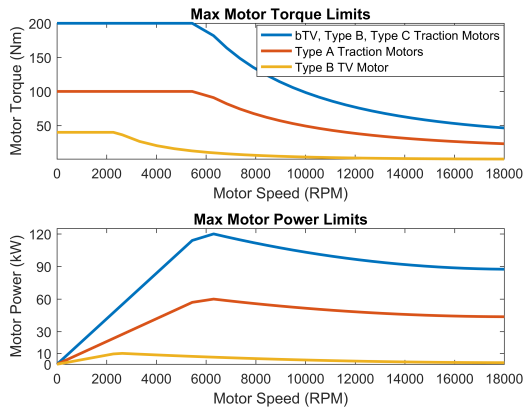

Fig. 11: Maximum motor torque and power limits as a function of motor speed

3) The total axle vectoring torque capability shall not be lower than 1600 Nm

In order to meet requirements 1 and 2, the gear ratio between the motor and the wheels is fixed at 10:1 for all of the systems. The baseline, Type B and Type C traction motors will be sized for a maximum torque of 200 Nm and a peak power of 120 kW. The Type A system will use two 60 kW motors with a maximum torque of 100 Nm each thus providing a combined power of 120 kW and 200 Nm. Fnally, in order to meet requirement 3, the vectoring motor of the Type B system will use a 10 kW motor with a maximum torque of 40 Nm and an effective gear ratio of 40:1 thus providing a maximum vectoring torque capability of 1600 Nm at the wheels. The maximum motor torque and power for each system is shown in fig. 11. As can be seen, the torque capability of each motor has a ”constant torque” region where maximum torque is achievable followed by a ”constant power” region where the power limits of the motor begin to limit the output torque as the motor speed increases. The maximum power plots show that the motor power begins to fall off once peak power is reached. This decrease in power is due to power losses baked into the model as the motor speed increases. The torque and power limits shown in fig. 11 will ensure a fair comparison between all of the eTV systems.

B. Test I: Constant Turn while Accelerating

The first test used in the study is light acceleration while in a constant turn. This simple test will give insight on how a continuous torque vectoring request will be affected while

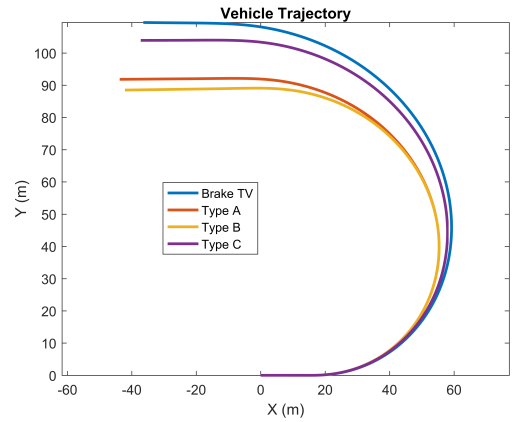

(a) Vehicle trajectory

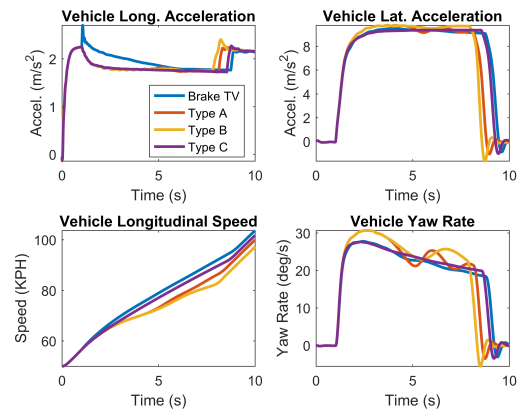

(b) Vehicle dynamics response

Fig. 12: Vehicle response for acceleration in turn test

the vehicle is accelerating. In order to maintain a fair comparison, a fixed 50/50 front/rear torque split is maintained for all of the systems. The only difference between the systems will be in how the rear axle distributes torque between the left and right wheels. In this test, the vehicle starts out with an initial speed of 50 KPH. At 0 seconds, a total wheel torque request of 1500 Nm is requested by the driver and is held constant throughout the entire test. Since the front/rear torque split is fixed to 50/50 for this study, each axle will need to deliver 750 Nm of traction torque. At 1 second, the driver applies a steering wheel input of 90 degrees and holds it until the vehicle makes a complete U-turn. The torque vectoring request is proportional to the driver’s steering wheel input until it reaches a maximum request of 1000 Nm.

Figure 12 shows the vehicle response for the four systems being analyzed. As can be seen from the vehicle trajectories in fig. 12a, the Type B system is able to make the tightest turn followed by the Type A system. The Type C system requires a much larger turning radius whereas the brake torque vectoring system requires the largest turning radius. It is worth noting that the Type A system has the flexibility to achieve the vectoring torque request in many different ways. However, in order to maintain the driver’s wheel

torque demand, the vectoring torque request was achieved by super-positioning the request in equal and opposite quantities on top of the traction torque request in a similar fashion to the Type B system. However, even though the Type A system employs the same super-positioning torque distribution strategy as the Type B system, it still requires a larger turning radius. Figure 12b shows that the type A and B systems obtain a larger yaw rate response from the vehicle and they tend to slow the vehicle down more than the Type C and brake torque vectoring systems. The reason for this is because the Type A and B systems cause a tighter turning radius thus leading to more tire scrub which naturally slows the vehicle down. One other noticeable difference in the vehicle response is the longitudinal acceleration of the brake torque vectoring system. There is an initial spike in longitudinal acceleration which can be explained by looking at the wheel torque response plots shown in fig. 13.

Figure 13 shows the motor torque and wheel torque response of each system. In fig. 13a, we can see that the control system automatically increases the traction motor torque request in conjunction with the vectoring torque request. This is done to make up for the torque that the friction brakes will be removing from the powertrain in order to maintain the driver's wheel torque request. Note that the initial brake rotor temperature is set to 60C. It is clear that the initial delivered braking torque on the left wheel does not meet the request due to the cold rotor temperature. As the rotor temperature warms up, the delivered braking torque finally meets the request. The initial difference between the delivered and requested brake torque is what causes the spike in vehicle acceleration - the powertrain was expecting the brakes to take away more torque than it actually did which resulted in a sudden spike in net wheel torque. It is also clear that as the vehicle accelerates, the traction motor transitions between the "constant torque" region to the "constant power" region. Therefore, the maximum torque capability of the motor begins to be clipped resulting in a total reduction of delivered vectoring torque capability as seen in Figure 13e. This explains why the brake torque vectoring system required the largest turning radius.

Figure 13b shows the motor torque inputs and the resulting wheel torque for the Type A system. It's clear from the plot that the vectoring torque request is split in equal and opposite quantities between the left and right wheels. However, as the vehicle accelerates, the right motor begins to enter the constant power region of the motor and the torque capability begins to drop off. In order to maintain the driver's wheel torque demand, the left motor torque is also reduced which causes the total delivered vectoring torque to drop off as seen in Figure 13e. The only way to continue delivering the requested vectoring torque request is to violate the rear axle traction torque request. In order to meet both the traction torque and vectoring torque request, the total traction torque request of the rear axle would need to be reduced and biased towards the front axle. This simple test tells us that in order to maintain the traction and vectoring torque request on a Type A system, additional coordination between the front and rear axle would need to take place.

We can now analyze the motor torque inputs and resulting wheel torques of the Type B system from fig. 13c. As can be seen, the traction motor applies 75 Nm to meet the rear axle traction torque request whereas the vectoring motor delivers 25 Nm to meet the vectoring torque request. The vectoring torque is distributed in equal and opposite quantities at the wheels and it is evident from fig. 13e that the Type B system is able to meet both the traction torque and vectoring torque request throughout the entire maneuver without any form of derating. The reason for this is because the traction motor speed is proportional to the average wheel speed whereas the vectoring motor speed is proportional to the wheel speed difference. It's clear that the traction motor enters the constant power region of the motor but the delivered motor torque is never clipped because the motor torque command is well below the max limits of the motor. The vectoring motor max torque limits are shown as a straight line thereby indicating that the motor is still operating in the constant torque region. The reason for this is because the wheel speed difference is quite small and it allows the vectoring motor to maintain full torque authority regardless of the actual vehicle speed. As can be seen from the system response, the Type B system offers a decoupled response that allows for decoupled control of the traction and vectoring torque. Furthermore, since the vectoring motor is only a function of the wheel speed difference, it allows the Type B system to maintain full vectoring torque capability at any vehicle speed. This test shows us that we can decouple the front and rear torque split from the vectoring torque capability which is an extremely important insight.

Next, we can analyze the Type C system by looking at fig. 13d and fig. 13e. From fig. 13e we can see that the system is able to fully meet the driver's wheel torque request but it can't fully meet the vectoring torque request. The reason for this is that the Type C system can only distribute the traction motor's torque between the left and right wheels. From fig. 13d we can see that the traction motor delivers 75 Nm to meet the rear axle traction torque request. When the vectoring torque request is applied, the Type C system biases the entire traction torque to the right wheel in order to try and meet the vectoring torque request. However, the torque command that is necessary to meet the rear axle traction torque request is not enough to fully meet the vectoring torque request. The only way to fix this problem is to increase the rear axle traction torque request i.e. bias more torque to the rear axle. In this way, the traction motor torque is increased and it will be able to meet both the traction and vectoring torque requests. This test tells us that the Type C system also needs additional coordination between the front and rear torque split in order to fully obtain the desired vectoring torque request.

Finally, fig. 13e shows how each system handled the driver's wheel torque request and vectoring torque request. For this study, meeting the driver's wheel torque request was prioritized. As can be seen, all four systems met the driver's wheel torque request with the brake torque vectoring system

having a small violation due to the brake torque response. The only system that was able to fully meet both the wheel torque and vectoring torque request is the Type B system. The rest of the systems were not able to fully meet the vectoring torque request and the only way that they would be able to is by having additional coordination with the front/rear torque split controls. Although the Type A system theoretically offers the most wheel torque control flexibility, the torque constraints imposed by motor power limits causes the system to lose a significant amount of performance. On the other hand, the Type B system is able to deliver good torque vectoring performance from its 10 kW motor due to the decoupled control capability. It is also worth noting that the vehicle speed ranged between 50-100 KPH during this test which is within the speed range vehicles operate in during normal driving cycles.

C. Test II: Off Pedal Constant Turn

The second and final test used in the study is a constant turn while at off pedal. This simple test will reveal how the different eTV technologies handle a continuous vectoring torque request when there is no wheel torque command from the driver. Similar to the acceleration in turn test, the vehicle starts out with an initial speed of 50 KPH. At 1 second, the driver applies a steering wheel input of 90 degrees and holds it until the vehicle makes a complete U-turn. The torque vectoring request is proportional to the driver's steering wheel input until it reaches a maximum request of 1000 Nm. Since the driver is off pedal, there is no wheel torque request from the driver throughout the entire maneuver.

Figure 14 summarizes the response of the four systems for this test. As seen from fig. 14f, the Type A and B systems have an identical vehicle trajectory and the tightest turning radius. The brake torque vectoring system comes in 2nd and the Type C system has the largest turning radius. The reason the Type C system performs poorly during this test can be explained by analyzing fig. 14d. Since the driver is off pedal, there is no traction torque command to the front or rear axles, thus, the Type C system does not have any traction torque to distribute between the left and right wheels. The only way to fix this is by coordinating the rear axle traction motor torque with the rear axle brakes in a similar fashion to the brake torque vectoring system. This test shows that additional coordination between the powertrain and braking system is required in order for the Type C system to be able to provide torque vectoring capability during off throttle maneuvers.

The brake torque vectoring system shown in fig. 14a shows a similar response to the acceleration case - the brakes don't fully deliver the requested braking torque until the brakes come up to temperature. As a result, the brake torque vectoring system has a sudden application of total wheel torque due to the powertrain delivering more torque than the brakes were able to take away. The end result is a slowly increasing vectoring torque which helps turn the vehicle in a tighter turning radius.

As is seen from fig. 14b,c, and e, the Type A and B systems provide an identical response but through a different set of control inputs. The Type A system applies the vectoring torque request with equal and opposite motor torque commands resulting in no net traction torque while delivering the desired vectoring torque. On the other hand, the Type B system uses the small vectoring motor to provide the desired vectoring torque response while maintaining a net traction torque of zero by not actuating the traction motor. The end result is a system that meets both the driver's wheel torque request of zero and the desired vectoring torque request.

It is important to note that from a driver's point of view, the off pedal vectoring response is extremely noticeable and rewarding. Therefore, having a system that can deliver consistent vectoring torque while both on and off pedal is extremely important to the driving characteristics of an eTV vehicle. The two simple tests analyzed in this study show the limitations of each system. From these tests, we can conclude that although the Type A system may offer the most flexibility in wheel torque application, the power limits of the motors can significantly limit the vectoring capability at mid to high vehicle speeds. On the other hand, the Type B system offers the best combination of vectoring and traction torque capability due to the decoupled nature of the system. Finally, the Type C system offers the most economical eTV solution at the cost of a coupled response between the traction and vectoring torque.

IV. Conclusions

This study analyzed three eTV technologies and compared them with a brake torque vectoring implementation as the baseline. Bond graph models of all four systems were derived and implemented in the simulation environment with a high fidelity vehicle dynamics model from CarSim. In order to have a fair comparison, the same nonlinear motor torque and power limits were imposed on all systems - 200 Nm of combined traction motor torque a combined peak power of 120 kW. Two simple tests were used to analyze the systems, a constant turn while accelerating and an off pedal constant turn both performed with an initial vehicle speed of 50 KPH.

The acceleration in turn test showed that the Type B system was able to deliver the tightest turning radius by meeting the driver's wheel torque and vectoring torque requests without compromise. On the other hand, as the vehicle speed increased, the motor power limits on the Type A system limited the amount of vectoring torque capability and the only way to remedy this problem is by reducing the traction torque request to the rear axle and shift it towards the front. The Type C system obtained the next tightest turning radius. However, the Type C system was not able to fully meet the driver's vectoring torque request because the available traction torque was not sufficiently large enough. The only way to fix this problem is by increasing the traction torque to the rear axle and biasing more torque to the rear. Finally, the brake torque vectoring system provided the largest turning radius. The brake torque vectoring system used a control strategy which coordinated the powertrain and friction brake torque in order to provide the vectoring torque functionality. This system was not able to fully meet the driver's vectoring

torque request until the brake temperature increased to it's optimal operating range. As a result, the delivered vectoring torque fell short of the request thus resulting in the largest turning radius. The acceleration in turn test showed that the Type A and C systems require additional coordination with the front/rear torque split controls in order to fully meet the vectoring torque requests at all times. On the other hand, the Type B system's decoupled response allows the vectoring torque to be completely independent of the front/rear torque split controls which is allows for better overall vectoring performance regardless of the vehicle speed.

The off-pedal constant turn test showed that the Type B and A systems were the only ones able to fully meet the driver's wheel torque and vectoring requests without compromise. However, The Type A system would again start to become power limited if the test were done at a faster starting speed. The Type C system was not able to provide any vectoring torque due to the wheel torque request of zero. Additional coordination between the powertrain and brake controls would be required in order for the Type C system to be able to deliver vectoring torque while not violating the driver's net wheel torque request of zero.

Overall, this study shows that the Type B system offers the best combination of traction and vectoring torque performance regardless of vehicle speed or acceleration. This is due to the decoupled nature of the system and the fact that the vectoring motor is only a function of the wheel speed difference and thus does not become power limited at higher vehicle speeds like the other two eTV systems.

ACKNOWLEDGMENT

The authors would like to thank Joe Torres and Peter Barrette from the Ford Transmission, Driveline & E-Drive Systems department for their contributions to this study.

REFERENCES

[1] L. Kakalis, A. Zorzutti, F. Cheli, and G. C. Travaglio, "Brake based torque vectoring for sport vehicle performance improvement," *SAE International Journal of Passenger Cars-Mechanical Systems*, vol. 1, no. 2008-01-0596, pp. 514–525, 2008.

[2] "Ford focus st product overview." [Online]. Available: https://media.ford.com/content/fordmedia/feu/gb/en/products/performance-cars/focus-st/focus-st.html

[3] J. Deur, V. Ivanović, M. Hancock, and F. Assadian, "Modeling and analysis of active differential dynamics," *Journal of dynamic systems, measurement, and control*, vol. 132, no. 6, 2010.

[4] J. V. Alcantar, F. Assadian, and M. Kuang, "Vehicle dynamics control of eawd hybrid electric vehicle using slip ratio optimization and allocation," *Journal of Dynamic Systems, Measurement, and Control*, vol. 140, no. 9, 2018.

[5] J. Y. Goh, T. Goel, and J. Christian Gerdes, "Toward automated vehicle control beyond the stability limits: drifting along a general path," *Journal of Dynamic Systems, Measurement, and Control*, vol. 142, no. 2, 2020.

[6] D. C. Karnopp, D. L. Margolis, and R. C. Rosenberg, *System dynamics: modeling, simulation, and control of mechatronic systems*. John Wiley & Sons, 2012.

[7] D. Hrovat and W. Tobler, "Bond graph modeling of automotive power trains," *Journal of the Franklin Institute*, vol. 328, no. 5, pp. 623–662, 1991.

[8] Mechanical simulation corporation, "Carsim." [Online]. Available: https://www.carsim.com

[9] H. B. Pacejka and E. Bakker, "The magic formula tyre model," *Vehicle system dynamics*, vol. 21, no. S1, pp. 1–18, 1992.

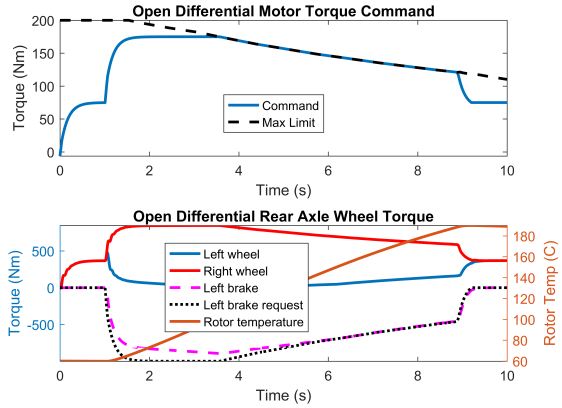

(a) Open differential with brake TV

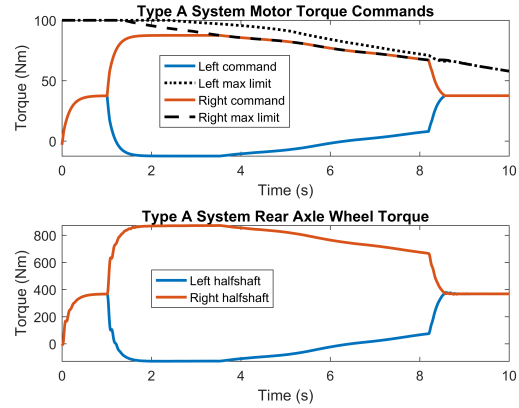

(b) Type A system

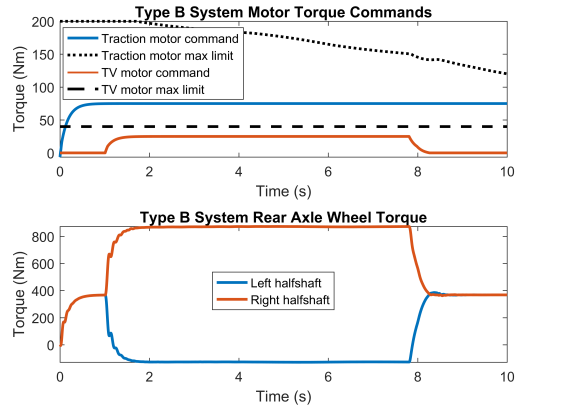

(c) Type B system

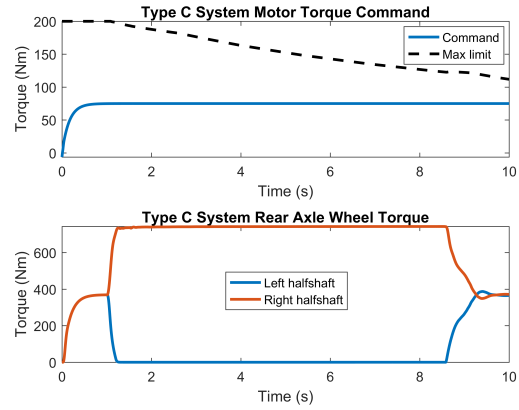

(d) Type C system

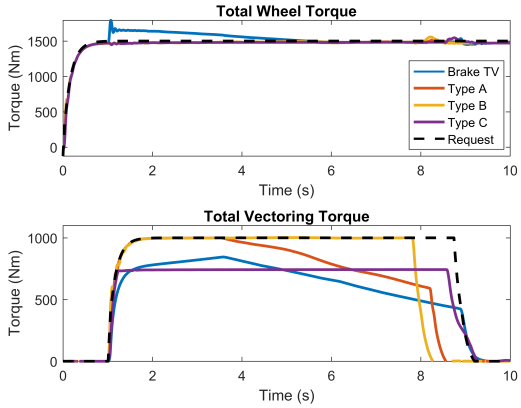

(e) Total wheel torque response

Fig. 13: eTV system response for acceleration in turn test

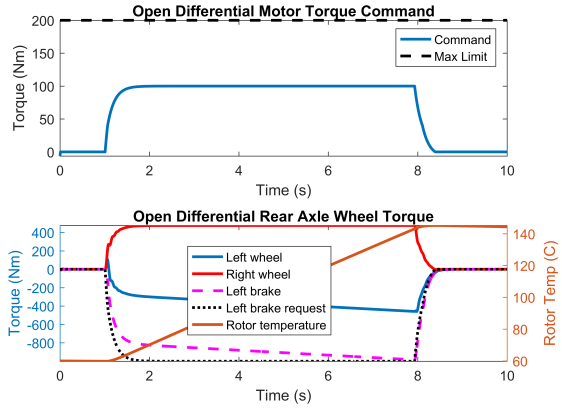

(a) Open differential with brake TV

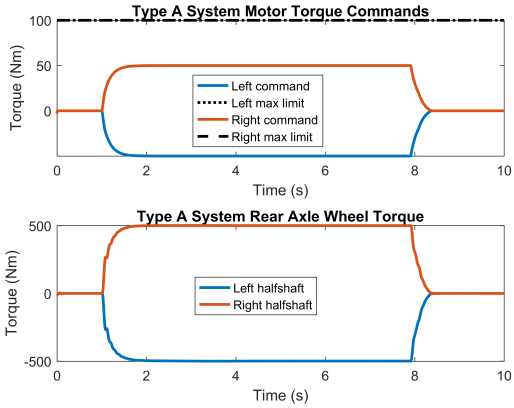

(b) Type A system

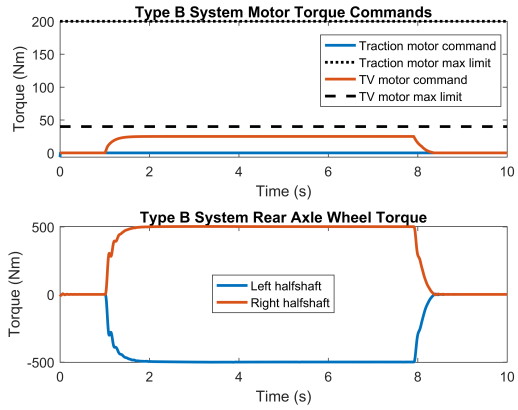

(c) Type B system

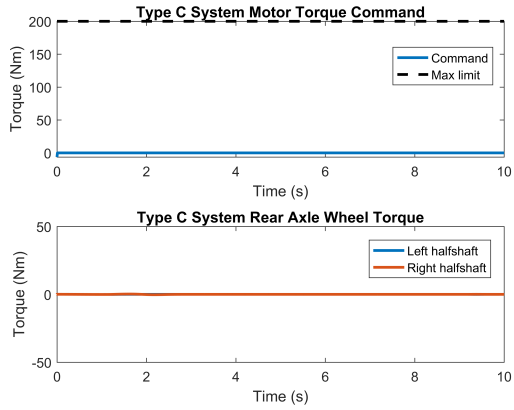

(d) Type C system

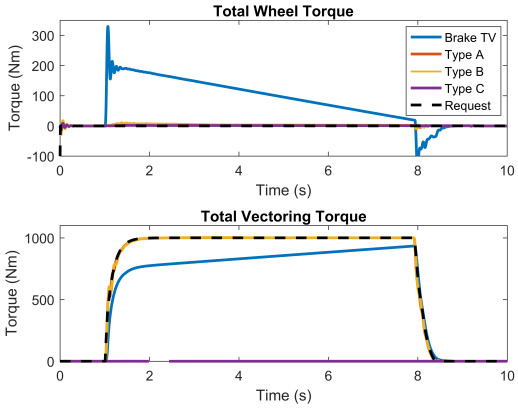

(e) Total wheel torque response

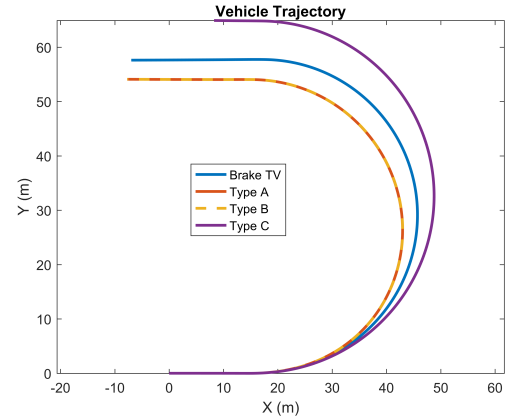

(f) Vehicle trajectory

Fig. 14: eTV system response for off pedal turn test